Supporting Information

Au nanoparticles induced localized surface plasmon resonance effect and synergistic catalytic sites in $Au/Co_3O_4/Si$ pyramid arrays for photoelectrochemical hydrogen evolution

Yu Wang, Chenyu Yan, Honggui Wang and Ya Zhang *

School of Environmental Science and Engineering, Institute of Technology for Carbon Neutralization, Yangzhou University, Yangzhou, Jiangsu, 225127, China.

*Corresponding author.

E-mail: zhangya@yzu.edu.cn (Y. Zhang).

Phone: +86-15366910300.

Materials and Reagents

Silicon wafers measuring 10×10 mm^2 were obtained from Zhejiang Huahe Silicon Material Co., Ltd. Chemicals such as sulfuric acid (H_2SO_4), hydrogen peroxide (H_2O_2), hydrofluoric acid (HF), potassium hydroxide (KOH), phosphorus oxychloride ($POCl_4$), ethylene glycol (EG), ethanol, and other reagents were purchased from Sinopharm Chemical Reagent Co., Ltd (Shanghai, China). Chemicals such as cobalt (II) nitrate hexahydrate ($Co(NO_3)_2 \cdot 6H_2O$) and potassium auric chloride ($KAuCl_4$) were purchased from Aladdin Co., Ltd. Ultrapure water with a resistivity greater than 18.2 $M\Omega \cdot cm^{-1}$ was used in this experiment. No further purification was performed on the compounds during the experiment.

Characterizations

Morphological observations of the material were performed on a Philips Tecnai G2 F30 S-TWIN high-resolution transmission electron microscope (HRTEM) and a HITACHI S-4800 field emission scanning electron microscopy (SEM), along with elemental mapping. X-ray diffraction (XRD) analysis was performed on a Bruker D8 X-ray diffractometer using Cu-Kα radiation (λ = 1.5406 Å) with a scattering range of 10° to 80° for 2θ, at a scan rate of 2° min^{-1}. Raman spectra were measured on an In Via laser confocal Raman spectrometer in turn. X-ray photoelectron spectroscopy (XPS) measurements were measured on a Thermo Scientific X-ray photoelectron spectroscopy system (ESCALAB 250Xi) with monochromatic Al Kα radiation (E = 1486.2 eV), and the binding energies were calibrated by C 1s to 284.8 eV. Oxygen

vacancies were measured by electron paramagnetic resonance (EPR) (BRUKER EMXPLUS). The UV-vis diffuse reflectance spectrum was obtained on the Varian Cary 5000 UV-vis near-infrared spectrophotometer. Atomic force microscopy (AFM) tests were measured on a Bruker's icon and use contactless mode. The ICP-MS measurement was studied on Agilent 720ES. Details of the experiment are as follows:

First, the mass of the samples Si/$Co_3O_4$1/Au, Si/$Co_3O_4$5/Au, Si/$Co_3O_4$10/Au were weighed with an analytical balance (to the nearest 0.0001 g), and transferred to three clean sample digestion cups. Then, 3 mL of hydrochloric acid and 1 mL of nitric acid were added and left at room temperature for 30 min. The samples were then heated for degradation by an electric heating digestion apparatus with a pre-set ramp-up program, and finally the samples were continuously digested at 200 °C for about 60 min. After digestion was complete, the digestion cup was removed and cooled naturally to room temperature. Finally, the digestion solution was transferred and filtered into a 10 mL volumetric flask and the digestion vessel was rinsed three times, then volumed with deionized water to 10 mL, mixed well and left to be measured.

Standard curve:

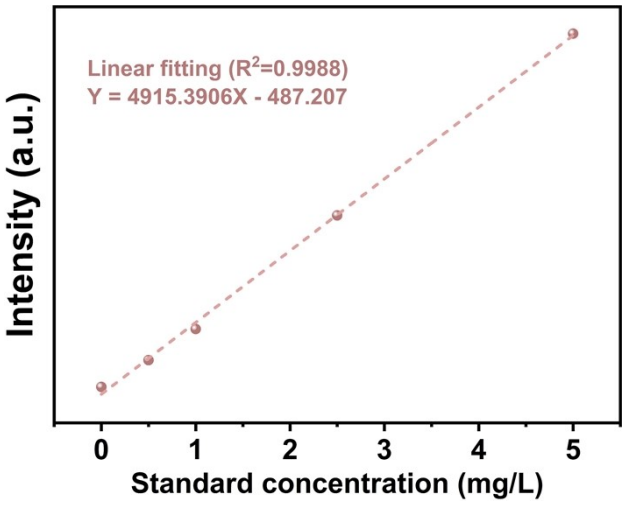

Element concentration of the sample digestion solution was calculated as follows:

$$C_1 = C_0 \times f \quad (1)$$

where C_0 (mg L^{-1}) is the concentration of elements in the solution and derived from instrument testing. f is the dilution ratio.

The final result of the measured element was calculated as follow:

$$C_X = \frac{C_1 \times V_0 \times 10^3}{m_0 \times 10^{-3}} \quad (2)$$

where m_0 (g) is the quality of the samples and recorded by analytical balance. V_0 (mL) is the volume of constant volume after sample digestion.

The final result of the measured element expressed as a percentage was calculated as follow:

$$W(\%) = \frac{C_x}{10^6} \times 100\% \quad (3)$$

Photoelectrochemical Measurements

The photoelectrochemical tests were conducted in a 0.5 M H_2SO_4 solution (pH = 0) on a CHI660D electrochemical workstation (Chenhua, Shanghai) with a three-electrode system consisting of the modified working electrode (WE), a saturated calomel electrode reference electrode (RE), and a graphite rod counter electrode (CE). The WE preparation method: Firstly, the oxide layer on the back of the silicon wafer is scraped with a blade and coated with a layer of Gallium/Indium eutectic alloy (≥99.99%, Sigma-Aldrich). Then, the copper wire with a diameter of 1 mm is linked to the back of the

silicon wafer through conductive silver paste. Finally, the back and side of the electrode are wrapped with epoxy resin glue. The working area of the WE was controlled to 1 cm^2. A 100 $mW \cdot cm^{-2}$ Xe light source (Perfect Light CHF-XM 500 coupled with an AM 1.5G filter) was used as a solar simulator. Linear sweep voltammograms (LSVs) measurements were conducted at a scan rate of 20 $mV \cdot s^{-1}$. Electrochemical impedance spectra (EIS) measurements were carried out at frequencies from 0.1 Hz to 100 kHz under 0 V (vs. RHE) with an amplitude of 10 mV. All tests were performed without iR correction. The production of hydrogen was obtained by a GC9790II gas chromatograph (GC) at 0 V (vs. RHE) under simulated AM 1.5G solar irradiation.

Calculation of H_2

Standard curve:

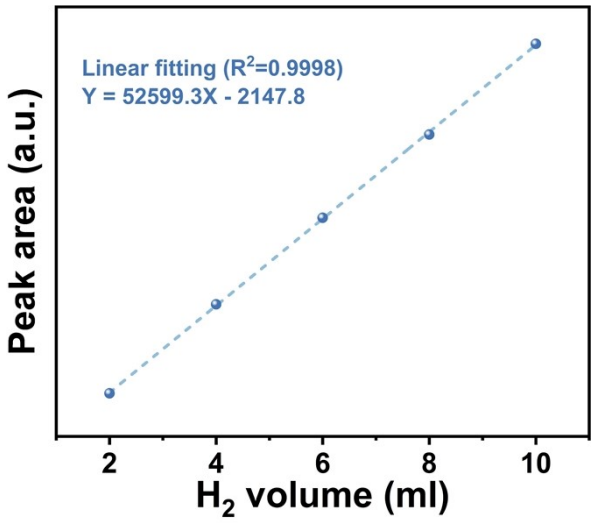

According to the standard curve, the peak area measured in the experiment can be substituted to calculate the volume of H_2 produced by the reaction, and the amount of H_2 substance can be obtained by dividing the H_2 volume by 22.4 $L \cdot mol^{-1}$. Hydrogen production rate can be obtained by dividing the amount of H_2 by the reaction time.

DFT theoretical calculations

Computational method

Calculations based on first-principles density functional theory (DFT), including molecular dynamics simulations were executed utilizing the Vienna Ab initio Simulation Package (VASP)[1] in conjunction with the Projector Augmented Wave (PAW) methodology[2]. The exchange-correlation functional was managed within the parameters of the Generalized Gradient Approximation (GGA), adopting the Perdew-Burke-Ernzerhof (PBE) functional[3]. The geometric relaxation was carried through until the forces acting on each atom were less than 0.03 eV $Å^{-1}$. The sampling of the Brillouin zone was conducted using a 2*2*1 k-point grid. To assure rigorous consistency, calculations were performed until the energy convergence threshold was less than 10^{-5} eV. To effectively isolate periodic structures and preclude their interaction, a vacuum buffer of 15 Å was inserted along the z-axis. The unit cell is defined by the lattice constants: a = 16.09170 Å, b = 11.37860 Å, and c = 19.41550 Å. $\alpha = \beta = \gamma = 90°$.

The free energy of the intermediates is calculated at zero potential and pH = 0,

$$\Delta G = \Delta E_{DFT} + \Delta ZPE - T\Delta S \quad (4)$$

where ΔE_{DFT}, ΔZPE and ΔS are the changes of the reaction energy obtained from DFT calculations, zero-point energy, and the changes of entropy from the initial state to the final state, respectively. T is temperature and the T of 298.15 K was used in all computations.

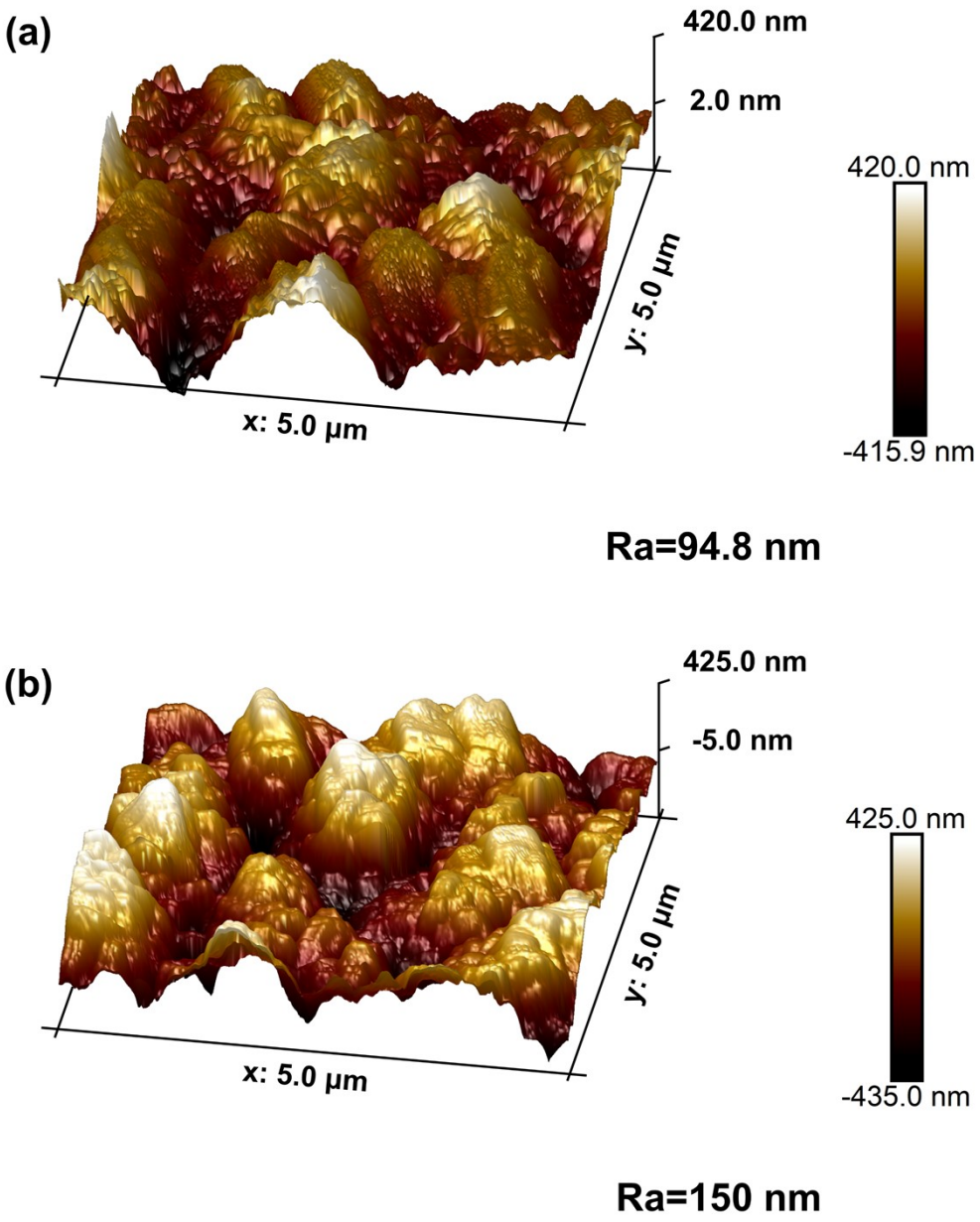

Fig. S1 3D topographic AFM images showing surfaces of (a) Si/Co_3O_4 and (b) Si/Co_3O_4/Au.

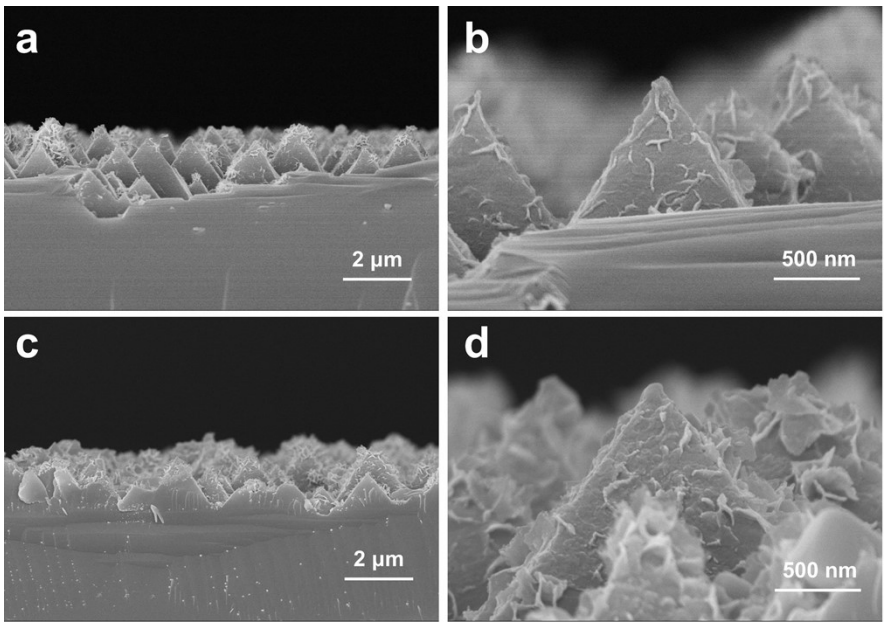

Fig. S2 (a), (b) Cross-sectional SEM images of Si/$Co_3O_4$1. (c), (d) Cross-sectional SEM images of Si/$Co_3O_4$1/Au.

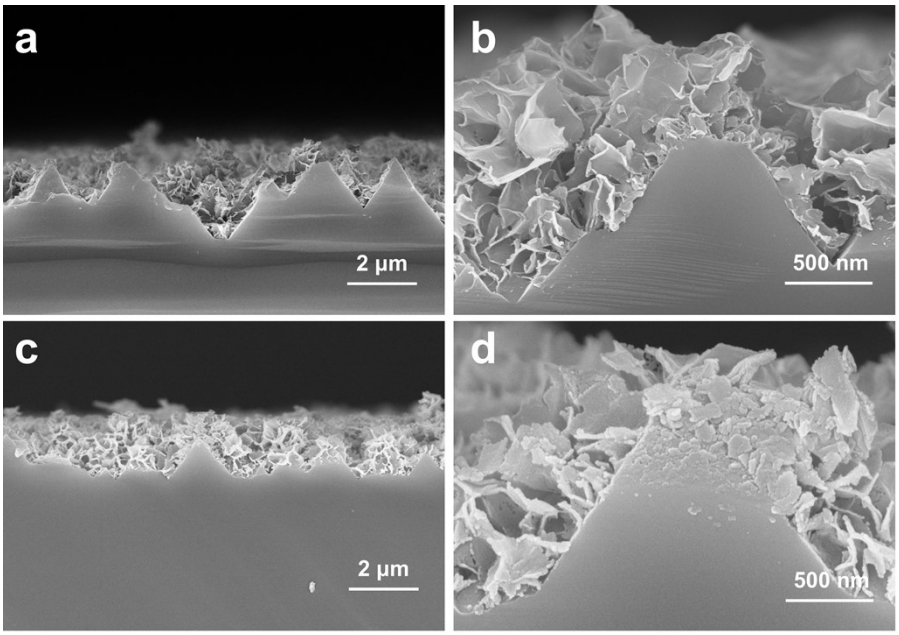

Fig. S3 (a), (b) Cross-sectional SEM images of Si/$Co_3O_4$10. (c), (d) Cross-sectional SEM images of Si/$Co_3O_4$10/Au.

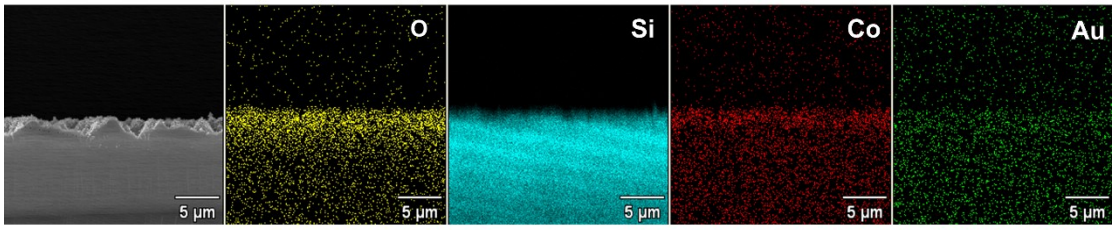

Fig. S4 EDX mapping image of the Si/Co_3O_4/Au.

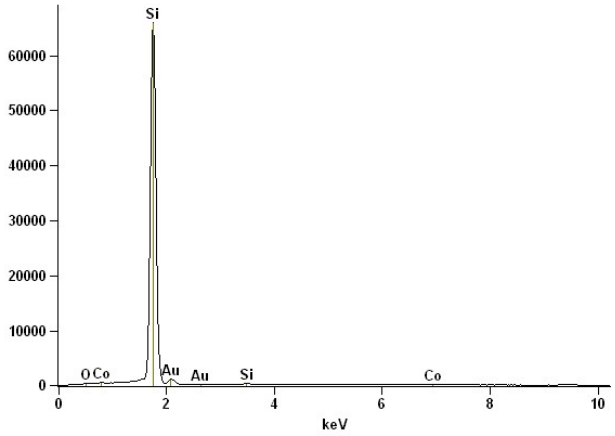

Fig. S5 EDX spectrum of the Si/Co_3O_4/Au.

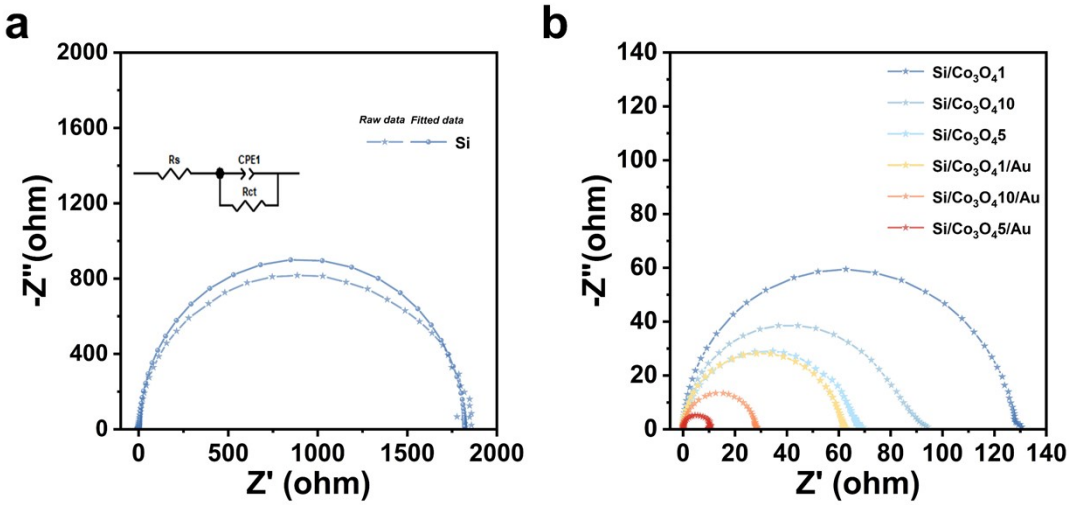

Fig. S6 (a) The electrochemical impedance spectra (EIS) raw data and fitted data of Si. (b) The EIS raw data of Si/Co_3O_4 and Si/Co_3O_4/Au with various electrodeposition times.

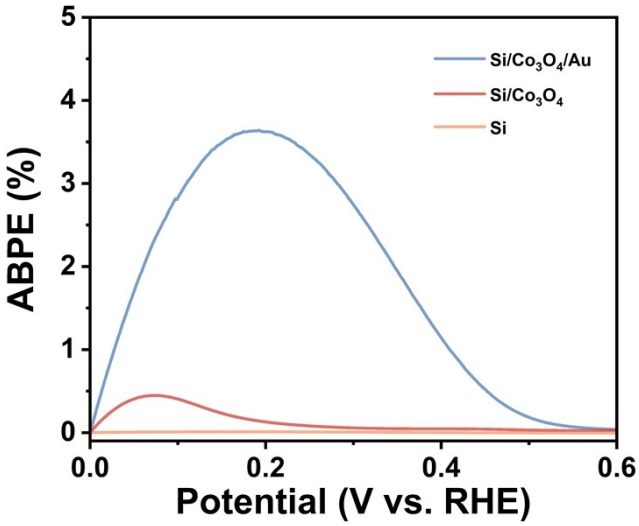

Fig. S7 ABPE curves of Si, Si/Co_3O_4, and $Si/Co_3O_4/Au$ in 0.5 M H_2SO_4 under simulated AM 1.5G solar irradiation.

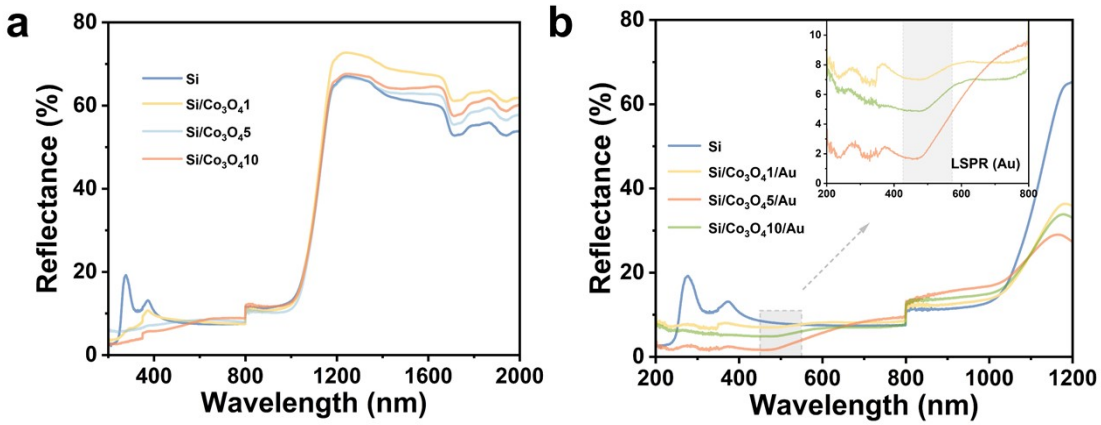

Fig. S8 UV−vis diffuse reflection of (a) Si/Co_3O_4 and (b) $Si/Co_3O_4/Au$ with various electrodeposition times.

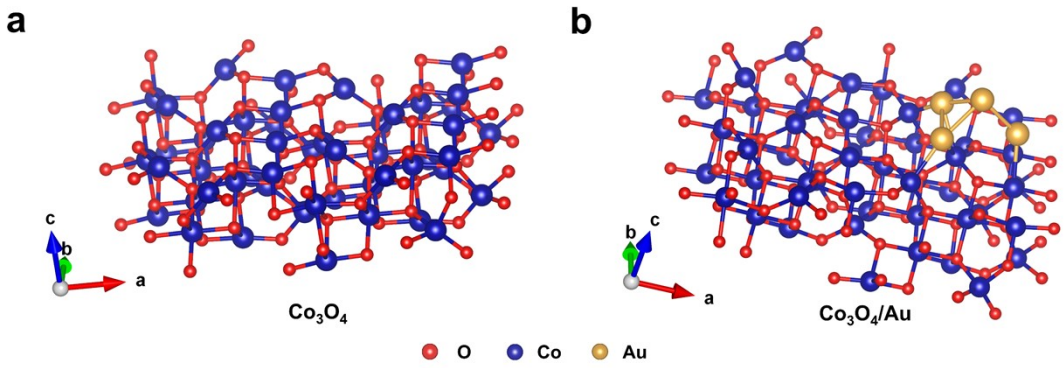

Fig. S9 Structural modelling diagrams of (a) Co_3O_4 and (b) Co_3O_4/Au.

Table S1. ICP-MS of Au concentration in different samples.

Samples	**Calibration volume** (mL)	**Au concentration of samples** (wt%)
Si/$Co_3O_4$1/Au	10	1.83
Si/$Co_3O_4$5/Au	10	2.06
Si/$Co_3O_4$10/Au	10	2.37

Table S2. Summary of PEC performance of state-of-the-art p-Si photocathodes.

Catalyst	Electrolyte	Irradiance	Onset potential (V vs. RHE)	J (mA/cm^2)	H_2 evolution rate	ABPE (%)	Refs.
$Si/Co_3O_4/Au$	**0.5 M H_2SO_4**	**100 $mW \cdot cm^{-2}$, AM 1.5 G**	**+0.42**	**-38.5@ 0 V_{RHE}**	**14.28 μmol min^{-1} cm^{-2}**	**3.7**	**This work**
n^+p-$Si/Nb_2O_5/NiPt$	0.5 M H_2SO_4	100 $mW \cdot cm^{-2}$, AM 1.5 G	+0.62	-32@ 0 V_{RHE}	130 μmol cm^{-2} in 5 h	5.2 @0.3 V_{RHE}	2023[4]
Co-W-S/Ti/n^+p-Si	1 M $HClO_4$	100 $mW \cdot cm^{-2}$, AM 1.5 G	+0.36	-30.4@ 0 V_{RHE}	/	4	2018[5]
$Si/rGO/MoS_2$	0.5 M H_2SO_4	100 $mW \cdot cm^{-2}$, AM 1.5 G	+0.38	-41.6@ 0 V_{RHE}	18.1 μmol cm^{-2} min^{-1}	3.4	2024[6]
n^+p-$Si/Ti/WO_3@RuSe_2$	0.5 M H_2SO_4	100 $mW \cdot cm^{-2}$	+0.54	-36@ 0 V_{RHE}	315 μmol in 3 h	9.43	2022[7]
n^+p-Si/Ti/Ru-MoS_2	N_2-saturated 0.5 M H_2SO_4	100 $mW \cdot cm^{-2}$, AM 1.5 G	+0.53	-43@ 0 V_{RHE}	280 μmol in 160 min	7.28 (HC-STH)	2021[8]
$MoS_2/TiO_2/Si$	0.5 M H_2SO_4	100 $mW \cdot cm^{-2}$, AM 1.5 G	+0.46	-33.7@ 0 V_{RHE}	10.5 μmol cm^{-2} min^{-1}	4.9	2021[9]
Ni/TiO_2/a-Si/n-c-Si/a-Si/ITO/TiO_2/Pt	1 M $HClO_4$ (pH=0)	AM 1.5 G	+0.62	-35@ 0 V_{RHE}	/	12.66	2020[10]
Si/Co–NCNHP–TiO_2/CoP	0.5 M H_2SO_4	100 $mW \cdot cm^{-2}$, AM 1.5 G	+0.409	-23.04@ 0 V_{RHE}	550 μmol cm^{-2} in 2 h	2.262	2024[11]
$Ni_{0.95}Pt_{0.05}Si$/p-Si	0.5 M H_2SO_4	100 $mW \cdot cm^{-2}$, AM 1.5 G	+0.45	-40.5@ 0 V_{RHE}	/	5.3	2023[12]
p-Si/In_2S_3/Pt	pH 5.7 phosphate buffer	AM 1.5 G	+0.5	-35@ -0.3 V_{RHE}	/	5.6 @0.25 V_{RHE}	2024[13]
SimPy/MoO_x	0.5 M Na_2SO_4 solution (pH adjusted to 1 with H_2SO_4)	100 $mW \cdot cm^{-2}$, AM 1.5 G	/	-35@ -0.4 V_{RHE}	11 μmol cm^{-2} min^{-1}	/	2017[14]
Pt/rGO/p-Si	0.5 M H_2SO_4	100 $mW \cdot cm^{-2}$, AM 1.5 G	+0.43	-30.3@ 0 V_{RHE}	3.8 mmol in 5 h	4.9	2022[15]
Si-MoS_2	0.5 M H_2SO_4 (pH=0)	100 $mW \cdot cm^{-2}$, AM 1.5 G	+0.25	-30@ 0 V_{RHE}	1.5 mmol in 3 h	/	2021[16]
Si–$MoSe_2$			+0.22	-26@ 0 V_{RHE}	0.6 mmol in 3 h	/	
Si–WS_2			+0.24	-23@ 0 V_{RHE}	1.2 mmol in 3 h	/	
Si–WSe_2			+0.18	-22@ 0 V_{RHE}	1.1 mmol in 3 h	/	
SiNW_AuCQDs	0.5 M H_2SO_4	100 $mW \cdot cm^{-2}$	/	-35.5@ -1.2 V_{RHE}	182.93 μmol·h^{-1}	6.1	2020[17]

SiNW/AuNP/MoS_2	0.5 M H_2SO_4	300 W xenon lamp with an AM 1.5 filter	+0.179	−14 @-0.5 V_{RHE}	246 mmol g^{-1} h^{-1}	/	2023[18]
TiO_2/AuNR/SiNHHN	0.5 M H_2SO_4	100 mW·cm^{-2}, AM 1.5 G	+0.32	−26.2 @-0.25 V_{RHE}	450 μmol·h^{-1}	/	2019[19]
MoO_x/p-Si	0.5 M H_2SO_4	100 mW·cm^{-2}, AM 1.5 G	/	−30 @-0.5 V_{RHE}	53 μmol g^{-1} h^{-1}	/	2019[20]

REFERENCES

1 G. Kresse and J. Furthmüller, *Comput. Mater. Sci.*, 1996, **6**, 15-50.

2 P. E. Blöchl, O. Jepsen and O. K. Andersen, *Phys. Rev. B*, 1994, **49**, 16223-16233.

3 J. P. Perdew, J. A. Chevary, S. H. Vosko, K. A. Jackson, M. R. Pederson, D. J. Singh and C. Fiolhais, *Phys. Rev. B*, 1993, **48**, 4978-4978.

4 M. Arunachalam, R. Subhash Kanase, J. Ganapati Badiger, S. Abdelfattah Sayed, K.-S. Ahn, J.-S. Ha, S.-W. Ryu and S. Hyung Kang, *Chem. Eng. J.*, 2023, **474**, 145262.

5 R. Fan, G. Huang, Y. Wang, Z. Mi and M. Shen, *Appl. Catal. B*, 2018, **237**, 158-165.

6 C. Yan, Z. Tang, L. Wang, Z. Piao, H. Wang and Y. Zhang, *Langmuir*, 2024, **40**, 12427-12436.

7 F. Zhang, X. Yu, Y. Qian, L. Qiu, Y. Xia, Y. Yao, Y. He, L. Lei, S. Hao and X. Zhang, *Chem. Eng. J.*, 2022, **446**, 137462.

8 F. Zhang, X. Yu, J. Hu, L. Lei, Y. He and X. Zhang, *Chem. Eng. J.*, 2021, **423**, 130231.

9 W. Xun, Y. Wang, R. Fan, Q. Mu, S. Ju, Y. Peng and M. Shen, *ACS Energy Lett.*, 2020, **6**, 267-276.

10 B. Liu, S. Feng, L. Yang, C. Li, Z. Luo, T. Wang and J. Gong, *Energy Environ. Sci.*, 2020, **13**, 221-228.

11 X. Li, H. Zhao, J. Huang, Y. Li, H. Miao, G. Shi and P. K. Wong, *J. Mater. Chem. A*, 2024, **12**, 16605-16616.

12 H. Zhang, S. Li, J. Xu, X. Sun, J. Xia, G. She, J. Yu, C. Ru, J. Luo, X. Meng, L.

Mu and W. Shi, *Small*, 2024, **20**, 2311738.

13 C. Ding, Y. Li, W. Xiao, Q. Chen, Y. Li, J. He and C. Li, *Int. J. Hydrogen Energy*, 2024, **66**, 40-47.

14 T. G. Truong, C. Mériadec, B. Fabre, J. F. Bergamini, O. de Sagazan, S. Ababou-Girard and G. Loget, *Nanoscale*, 2017, **9**, 1799-1804.

15 J. Shen, Y. Wang, C. Chen, Z. Wei, P. Song, S. Zou, W. Dong, X. Su, Y. Peng, R. Fan and M. Shen, *Appl. Phys. Lett.*, 2022, **121**, 213901.

16 I. H. Kwak, I. S. Kwon, J. H. Lee, Y. R. Lim and J. Park, *J. Mater. Chem. C*, 2021, **9**, 101-109.

17 D. Ghosh, K. Roy, K. Sarkar, P. Devi and P. Kumar, *ACS Appl. Mater. Interfaces*, 2020, **12**, 28792-28800.

18 C. Y. Chen, C. H. Mao, K. Y. Hsiao, Y. S. Huang, L. J. Chen, M. Y. Lu, T. Tanaka and T. J. Yen, *Solar RRL*, 2024, **8**, 2300821.

19 L. Zhang, X. Chen, Z. Hao, X. Chen, Y. Li, Y. Cui, C. Yuan and H. Ge, *ACS Appl. Nano Mater.*, 2019, **2**, 3654-3661.

20 I.-H. Yoo, Y.-J. Lee, S. S. Kalanur and H. Seo, *Appl. Catal. B*, 2020, **264**, 118542.